ELSEVIER

Analytica Chimica Acta 476 (2003) 93–109

ANALYTICA CHIMICA ACTA

www.elsevier.com/locate/aca

Application of modified alternating least squares regression to spectroscopic image analysis

Ji-Hong Wang [a], Philip K. Hopke [a,*], Thomas M. Hancewicz [b], Shuliang L. Zhang [b]

[a] *Department of Chemical Engineering, Clarkson University, Potsdam, NY 13699-5705, USA*
[b] *Unilever Research US, Edgewater, NJ 0702, USA*

Received 8 May 2002; received in revised form 3 October 2002; accepted 21 October 2002

Abstract

Analysis of synthetically generated and real Raman imaging data sets were used to show the significance of modified alternating least squares (MALS) regression as a superior method of analysis compared with several other well established mathematical algorithms. The performance of MALS was compared with that of ordinary alternating least squares regression (ALS) and fast non-negative least squares (FNNLS) regression in applications of spectroscopic image analysis and self-modeling curve resolution (SMCR). The MALS algorithm is shown to be superior in terms of computational speed, stability, and component resolution ability in the analysis of both real and synthetic data sets. Results of the analysis show that MALS is significantly faster than FNNLS and generally produces equivalent or superior results. This work also shows that MALS is superior to ordinary ALS in all performance aspects. A detailed description of the regression equations is given along with a discussion of the application of MALS to the general spectroscopic image analysis problem.

Keywords: Alternating least squares (ALS); Modified alternating least squares (MALS); Non-negativity; Ridge regression; Forced zero point ALS; Fast non-negative least squares (FNNLS)

1. Introduction

One of the most important software tools used to analyze and extract information from spectroscopic imaging data is self-modeling curve resolution (SMCR). This is standard methodology used in the physical and biological sciences and has been developed over the past several decades as a general component resolution tool [1–4]. The heart of SMCR methods is some form of alternating regression algorithm, which is used to refine initial estimates of a two- or three-way, bilinear data structure to an optimum least squares result. There are many forms of ALS used to solve such models but the most widely use is forced zero point ALS which simply sets negative values to zero in each step of the least squares iteration process. Thus, alternating least squares regression (ALS) is rapidly becoming the most commonly used method to solve spectroscopic image analysis problems based on either a bilinear and trilinear data model, the former being the most prevalent model. The method is reasonably fast for large data sets and produces reliable results [2,3]. However, ALS suffers from a number of potentially serious drawbacks that can significantly degrade performance and reliability for many types of imaging data sets. Chief

* Corresponding author. Tel.: +1-315-268-3861; fax: +1-315-268-6654.
E-mail address: hopkepk@clarkson.edu (P.K. Hopke).

0003-2670/02/$ – see front matter
PII: S0003-2670(02)01369-7

among these is slow processing speed due to convergence problems and high sensitivity to near-collinear data. When used for constrained least squares (LS) models incorporating either non-negativity or unimodality [4], ALS can be extremely slow to converge even if each individual iteration is relatively fast.

The *defacto* standard for solving non-negative LS problems has been the non-negative least squares (NNLS) method first introduced by Lawson and Hansen [5]. Bro and de Jong later improved this method as a fast non-negativity constrained least squares algorithm (FNNLS) [6]. This later method significantly improves the speed of NNLS, but it can still be prohibitively slow for very large problems even when implemented in the most computationally efficient manner possible. More recently methods that solve the non-negative LS problem using weighted LS optimization methods such have proven to be the most reliable and robust, but implementation of these methods can be difficult for those unfamiliar with the techniques [7,8]. One of these methods, Equation Oriented System, was used a referee method in this study [7]. The MALS method described in this paper is a solution to the constrained non-negative least squares problem for spectroscopic image analysis applications that is fast, accurate and robust. MALS is particularly appealing as a general method because it overcomes the problems associated with ALS and FNNLS.

2. Theory

2.1. The spectroscopic imaging problem

A typical spectroscopic image data set consists of a spectrum associated with each *X*, *Y* spatial dimensions on an image. This gives a three-dimensional problem that numerically is really a two-dimensional problem because the spatial dimensions are correlated. Spatial information is not used in the solution to the problem. It is also possible to collect imaging data as a spectrum at each point in three spatial dimensions but the solution still reduces to a two-dimensional problem although a quasi-trilinear solution is also possible for this special case. The 2D spatial case will be the only problem considered in this report but the methodology can easily be extrapolated to the 3D spatial case.

Spectroscopic imaging data can be collected in one of three ways: (1) spectroscopic mapping—a full spectrum is collected at each spatial point of an image map, (2) multi-wavelength imaging—a full 2D image is collected for each spectroscopic dimension (usually wavelength or wavenumber), (3) global imaging—a full spectral 2D image is collected simultaneously over all planar spatial dimensions. Regardless of the method of data collection, the inherent data structure is bilinear and assumes that some form of a Beer–Lambert relationship exists between spectral intensity and concentration [1]. Fig. 1 shows the process and data structure for the first two methods.

2.2. Alternating least squares (ALS)

2.2.1. ALS algorithm

The bilinear model can be expressed as

$$X = AB \tag{1}$$

where A and B are unknown factors to be estimated, and X is a measured data set. In spectroscopic imaging data, A will be the normalized spectra of pure chemical components and B will be the associated intensity information for each component (uncalibrated, but quantitative). Eq. (1) leads directly to the following two equations for the least squares estimation of A and B:

$$A = (XB^{\mathrm{T}})(BB^{\mathrm{T}})^{-1} \tag{1a}$$

$$B = (A^{\mathrm{T}}A)^{-1}(A^{\mathrm{T}}X). \tag{1b}$$

X, A and B are matrices of size m by n, m by p and p by n, respectively, where m, n, and p represent the number of spectroscopic resolution elements (i.e. wavelengths), total number of spectra (i.e. number of spatial resolution elements), and number of resolvable components, respectively. The objective of the analysis is to separate the contribution of each real component in X_n as A_n and B_n, so that $X_n = A_n B_n$ and $X = \Sigma X_n$. This is a two-way, bilinear model. The ALS method is a straightforward regression problem where initial estimates for A and B are generated initially using either random numbers, eigenvalue decomposition, or dissimilarity criterion [1]. In all examples used in this report the non-linear iterative partial least squares (NIPALS) decomposition method was used to generate initial estimates for A and B because it is

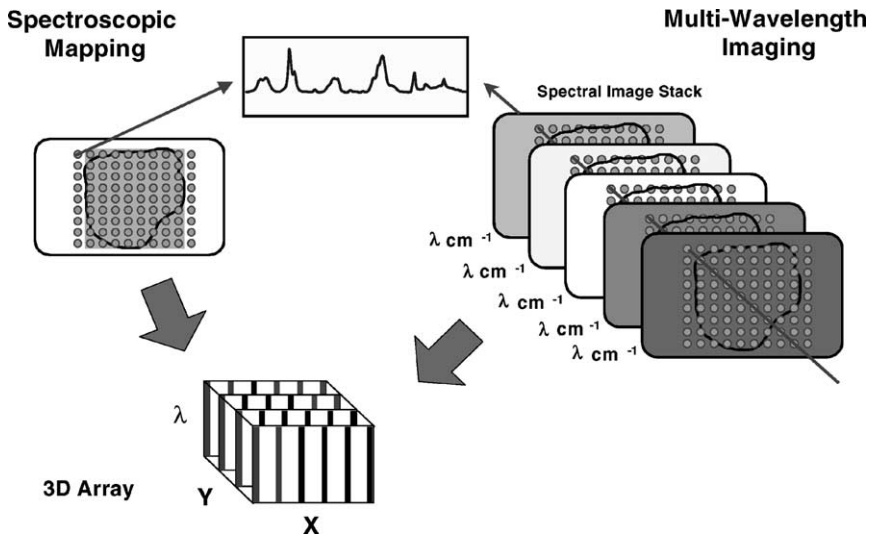

Fig. 1. The two most common spectroscopic image acquisition methods. The left diagram shows spectroscopic mapping and the right diagram shows multi-wavelength imaging. The two methods produce the same type of data set.

fast and provides a good numerical starting point for ALS.

2.2.2. ALS algorithm implementation

The ALS algorithm for solving Eq. (1) with non-negativity and two-norm equality constraints is given below as MATLAB code where A^{old} and B^{old} are the estimated factors:

1. Set the value of X and A^{old}.
2. Calculate the new estimate of B from X and A^{old}:
   - 2a. Normalize each column of A^{old} to Euclidean norm.
   - 2b. $A^{old} = \max(A^{old}, 0)$ (set negative values to zero).
   - 2c. $B^{new} = ((A^{old})^{T} A^{old})^{-1}((A^{old})^{T}X)$ (generate new LS estimate of B).
3. Calculate the new estimate of A from X and B^{old}:
   - 3a. $B^{old} = \max(B^{old}, 0)$ (set negative values to zero).
   - 3b. $A^{new} = (X(B^{old})^{T})(B^{old} (B^{old})^{T})^{-1}$ (generate new LS estimate of A).
4. Repeat steps (2) and (3) until convergence criterion is reached.

The general SMCR process for spectroscopic image analysis is show in Fig. 2.

2.3. Modified alternating least squares (MALS)

2.3.1. MALS algorithm

The idea behind the MALS algorithm is to modify the LS format used in the ordinary ALS algorithm. This modification amounts to the addition of two terms to the ordinary least squares equations for the ALS procedure. The first term transforms ALS into a ridge-regression (RR) algorithm. This allows the LS solution to be robust with respect to collinear data. The second term compensates for the inherent bias applied when forming the RR equations. This second term adds additional stability to the least squares regression for the boundary valued solutions sought in SMCR problems. The two terms together give this new method the advantages of RR without introduction of a bias term as in the typical RR method. Eqs. (1a) and (1b) are now replaced with modified expressions for the estimate of A and B. The following is the derivation of the MALS expression for A^{new} by fixing X and B^{old}:

$$A^{new} = (X(B^{old})^{T})(B^{old}(B^{old})^{T})^{-1} \quad (2)$$

rearranging Eq. (2):

$$X(B^{old})^{T} = A^{new}(B^{old}(B^{old})^{T}). \quad (3)$$

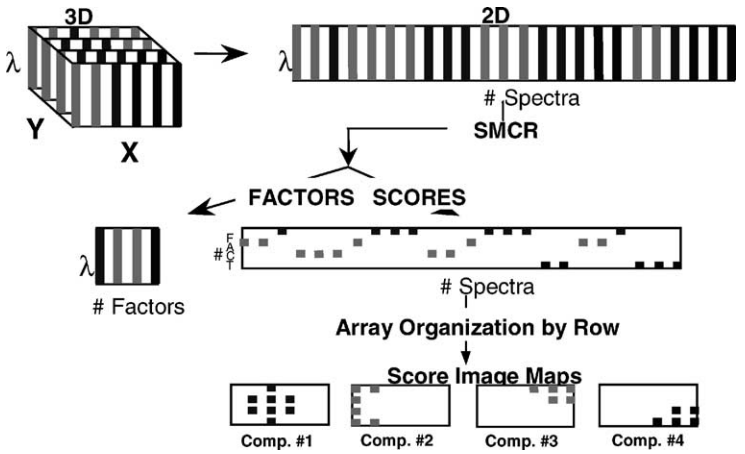

Fig. 2. Diagrammatic overview of spectroscopic image analysis process using self-modeling curve resolution (SMCR).

The ridge regression solution is applied by changing Eq. (2) as:

$$A^{\text{new}} = (X(B^{\text{old}})^{\text{T}})(B^{\text{old}}(B^{\text{old}})^{\text{T}} + W_{\text{a}})^{-1} \quad (4)$$

where W_{a} is a diagonal weight matrix of size p by p. The weight term is added to the right side of the expression. Eq. (4) is rearranged in the same way as Eq. (3) giving:

$$X(B^{\text{old}})^{\text{T}} = A^{\text{new}}(B^{\text{old}}(B^{\text{old}})^{\text{T}}) + A^{\text{new}}W_{\text{a}}. \quad (5)$$

Eq. (5) as written, does not hold unless W_{a} or A^{new} is equal to zero. A^{new} cannot equal zero since it is one of the quantities we are trying to determine, so that requires W_{a} to be as small as possible. This is the ridge-regression solution but as such it is not an acceptable solution for SMCR applications because it introduces a bias given by $A^{\text{new}}W_{\text{a}}$. If W_{a} is large, then a significant bias is introduced into the LS regression estimators leading to a solution that is uninterpretable. So, W_{a} should be chosen to be as small as possible.

However, it is desirable to avoid the bias problem if at all possible. One way to accomplish this is to modify Eq. (5) by adding the same bias term to the left side of the equation:

$$X(B^{\text{old}})^{\text{T}} + A^{\text{new}}W_{\text{a}} = A^{\text{new}}(B^{\text{old}}(B^{\text{old}})^{\text{T}}) + A^{\text{new}}W_{\text{a}}. \quad (6)$$

Now the expression as shown in Eq. (6) does not change the solution to Eq. (3), but this introduces a different problem to the LS solution. It now becomes very complicated mathematically to estimate A^{new} in a true LS sense because A^{new} is still an unknown quantity. The simplest way to solve this mathematically is to replace A^{new} on the left side of Eq. (6) with A^{old}, the previous estimate of A^{new} which is a known quantity:

$$X(B^{\text{old}})^{\text{T}} + A^{\text{old}}W_{\text{a}} = A^{\text{new}}(B^{\text{old}}(B^{\text{old}})^{\text{T}}) + A^{\text{new}}W_{\text{a}}. \quad (7)$$

Now an estimate of A^{new} is easily obtained from Eq. (7) by the following rearrangement:

$$A^{\text{new}} = (X(B^{\text{old}})^{\text{T}} + A^{\text{old}}W_{\text{a}})(B^{\text{old}}(B^{\text{old}})^{\text{T}} + W_{\text{a}})^{-1}. \quad (8)$$

Initially a small bias will still exist in the solution to Eq. (8). The magnitude of the bias is a function of the difference between A^{new} and A^{old}. However, as the LS solution tends toward convergence, this difference will become smaller and smaller until it is zero or insignificantly small at the time of convergence. There is no significant bias then by the time the LS solution converges. This now changes the previous RR restriction on the magnitude of W_{a}. Large values for W_{a} can now be used if desired because the bias will disappear by the time the solution converges. This fact has a very unexpected and powerful benefit to the LS solution. If W_{a} is large in the beginning it stabilizes the LS solution by slowing down the rate of convergence while only sacrificing a small amount of speed. In practical

terms this means the LS solution will tend not to get trapped in a local minimum and will generally converge on a global LS solution.

The estimation of B^{new} can be obtained in an analogous way to that shown above for A^{new}:

$$B^{new} = ((A^{old})^T A^{old} + W_b)^{-1}((A^{old})^T X + W_b B^{old}) \quad (9)$$

where W_b is also a diagonal weight matrix of size p by p.

2.3.2. Weights

There are many useful ways to set the weight values for MALS. In our research efforts we have looked at four different ways this might be accomplished:

(1) constant value based on the initial $||A||$ and $||B||$;
(2) linear change (increase or decrease) with iteration number;
(3) percentage of $||A||$ and $||B||$ at each iteration;
(4) percentage of $||A(a_{mp} < 0)||$ and $||B(b_{pn} < 0)||$ at each iteration.

The first two methods are not particularly suitable for spectroscopic imaging applications because they tend to either over-compensate or under-compensate for large variations in A and B. The third method works well in some situations but is not generally suitable for all problems. It tends to over-compensate in situations where the negative values in A or B are small even though $||A||$ and $||B||$ are large. The last method is perhaps the best for non-negativity constrained problems because it overcomes the deficiencies described for the last method. It sets the weights based on the magnitude of the negative values in A and B. This is intuitively reasonable since the rotation process is driven mainly by the non-negativity constraint.

One of the key features in our implementation of MALS is dynamic weight adjustment. While it is perfectly acceptable to apply weights based on a fixed percentage of the magnitude of A or B, it is our experience with spectroscopic imaging data that this is not the best approach. Indeed, in our first implementation of MALS we used fixed weights or percentages of fixed weights. The reality is that weight adjustment is a very delicate matter and deserves serious consideration. The reason for such care is in the balancing act required for optimal performance. As was stated earlier, perhaps in a slightly different way, the trade-off is speed of execution/convergence and stability of the solution with each iteration of the algorithm. It is typically desirable to set high weights in the very early iterations so large changes are made. The weights are adjusted according to the difference in magnitude of negative values in successive iterations between the current and previous estimate of the factors. This means that W_a and W_b may vary in very different ways from each other. In general, since the difference between iterations becomes smaller as the number of iterations increases and the magnitude of negative values becomes small, the weights will eventually converge on a fixed value. At the end of the analysis the weights are nearly constant.

It is sometimes useful to use a hybrid-weighting scheme where several different weighting methods are employed at different times during the LS optimization. In the analysis of most spectroscopic imaging data no weighting is required in the initial iterations because the negative values in A and B are sufficiently large and the solution converges monotonically. As the solution begins to stabilize, this condition is no longer true and weighting is required to maintain a stable convergence. A hybrid method is used in the current implementation of MALS and for all MALS analyses discussed in this report. The hybrid method uses no weighting in the initial few LS iterations (the standard ALS result) and thereafter dynamic weighting is used based on the difference in magnitude of negative values in A and B between successive iterations.

Fig. 3 shows a plot of the weight values versus iteration number for an example of Raman image analysis using MALS with the hybrid weighting scheme described above. It is clear that weight adjustment early in the analysis is most critical while adjustment toward the end is less important.

2.3.3. MALS algorithm implementation

The MALS algorithm for solving Eq. (1) is given as:

1. Set the value of X, A^{old} and B^{old}.
2. Calculate the new estimate of B from X, A, and B^{old}:
   2a. Normalize each column of A to Euclidean norm.
   2b. $A = \max(A, 0)$, (set negative values to zero).

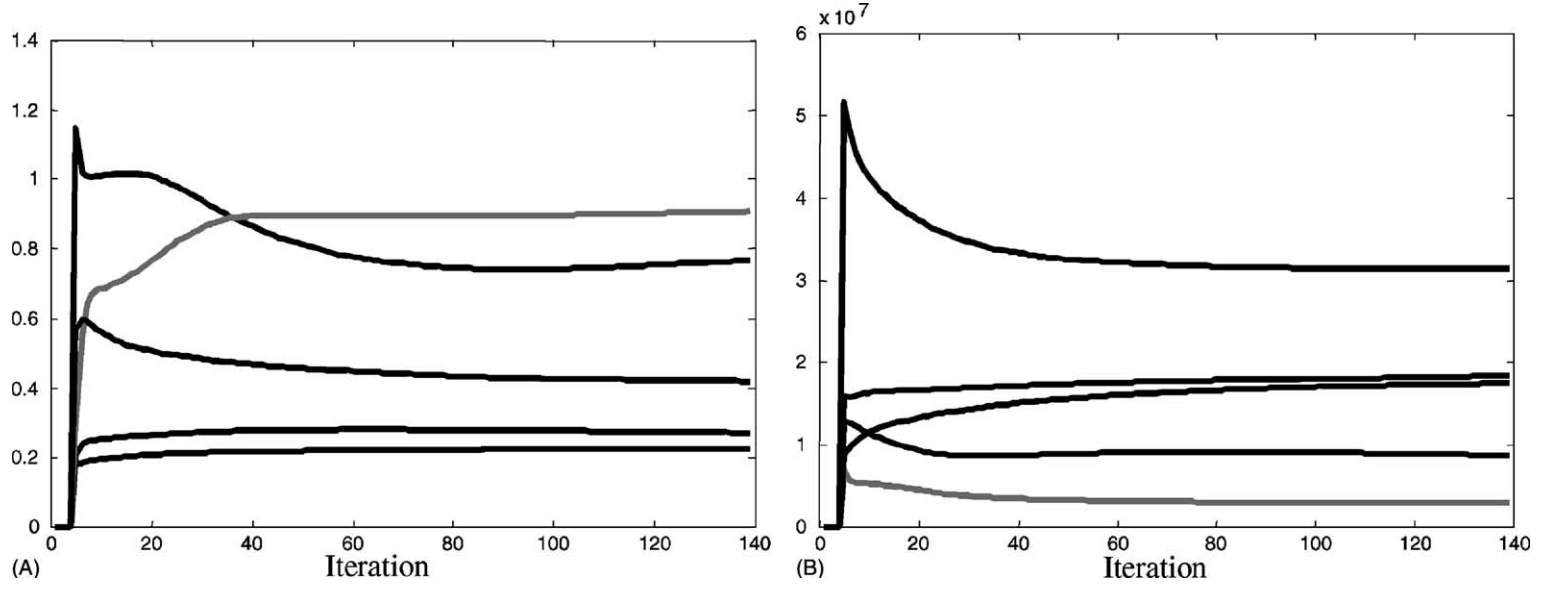

Fig. 3. Dynamic adjustment of MALS weights during LS optimization of a typical Raman image data set. The left plot (A) shows weights for spectra, W_a, while the right plot (B) shows the weights for Raman intensity matrix, W_b. The five curves in each box are for five components in the analysis.

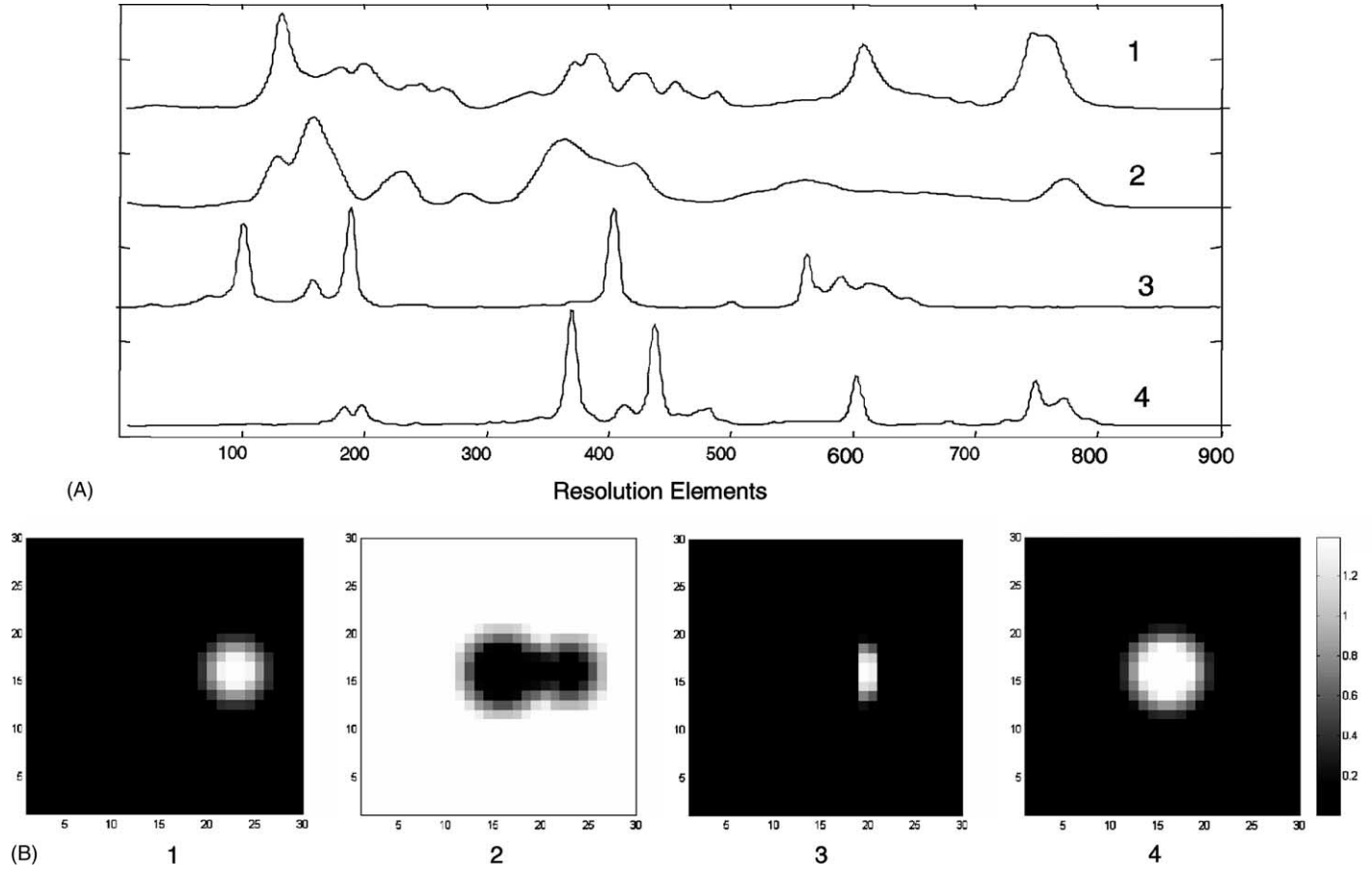

Fig. 4. (A) The spectral profiles used for synthetic data set (4×901 points); (B) The false images used with each of the four profiles in matrix A (30×30 points).

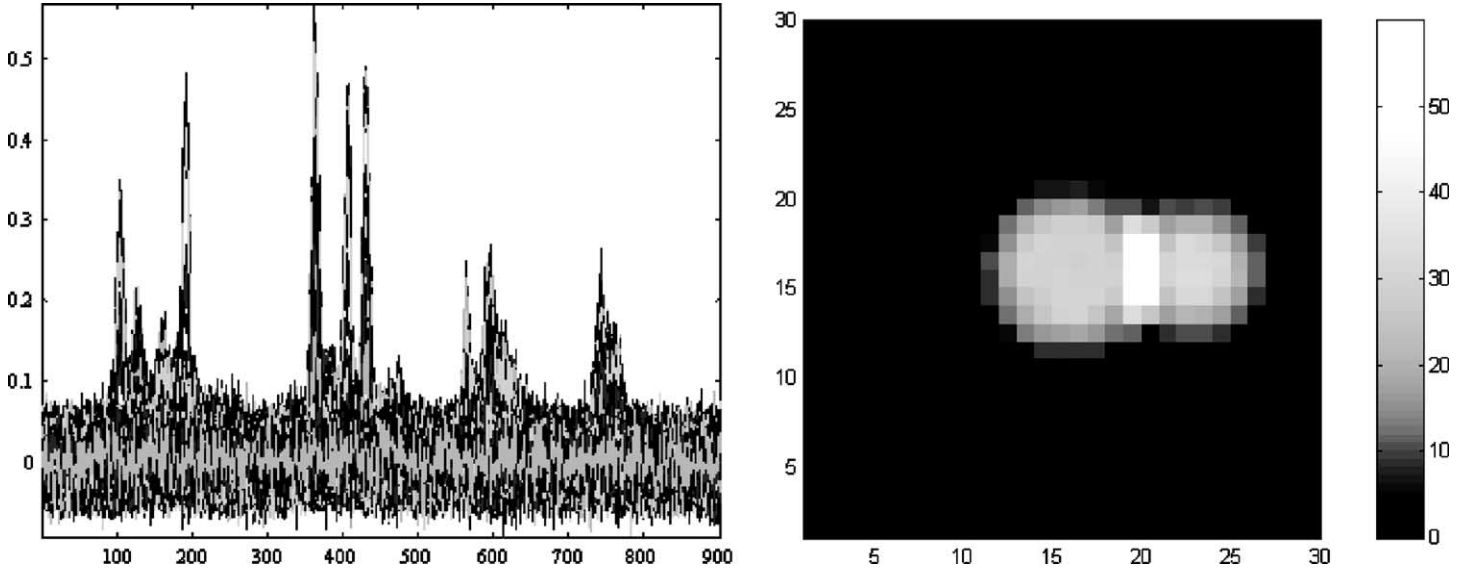

Fig. 5. Overlaid spectra and composite wavelength image of synthetically created “Raman image”. The data set is composed of 900 × 901 points spectra (left) for a 30 pixel × 30 pixel image (right).

2c. Set W_b.
2d. $B^{new} = (A^T A + W_b)^{-1} (A^T X + W_b B^{old})$.
2e. Set $B = B^{new}$; $A^{old} = A$.

3. Calculate the new estimation of A from X, B, and A^{old}:
   3a. $B = \max(B, 0)$, (set negative values to zero).
   3b. Set W_a.
   3c. $A^{new} = (XB^T + A^{old} W_a)(B B^T + W_a)^{-1}$.
   3d. Set $A = A^{new}$; $B^{old} = B$.
4. Repeat steps (2) and (3) until the convergence criterion is reached.

2.3.4. Fast non-negative least squares (FNNLS)

A detailed description of the FNNLS algorithm is beyond the scope of this report, but a summary of the idea behind the algorithm is included for completeness. Since the MALS algorithm will be compared with FNNLS for purposes of judging performance of the algorithm, some mention of it is required. FNNLS is considered by many to be the standard method for solving non-negative LS problems. It supersedes the non-negative least squares (NNLS) method first introduced by Lawson and Hansen [5] and is an improvement by Bro and de Jong [6] on the original algorithm. This later method significantly improves the speed of NNLS, but it can still be prohibitively slow for very large problems.

The basic idea of the FNNLS algorithm is to form the LS solution in terms of two sets of regression coefficients, an active set and a passive set. The set designation determines which data points will be directly constrained in the computation and which ones will not. As the names suggest, the active set is directly involved in the LS computation while the passive set is not. This is achieved through partitioning of the regression coefficients. The reason for this segregation of coefficients is so the solution will be a true least squares solution and not a conditional or approximate LS solution as would otherwise be the case. One reason the ALS algorithm is not so robust is because it applies the non-negativity constraint to all negative points in the data set regardless of if they need to be or not. Since the objective is to push the LS solution to a non-negative result, the true least squares solution should constrain only those points that would remain negative if no constraint was applied. If all the negative points are included in the computation then the LS solution becomes approximate and a less than optimum solution results. This is acceptable for many problems but is not usually desirable; particularly when the solution is nearly degenerate in several factors.

3. Experimental

Two data sets were used in evaluating MALS for spectroscopic image analysis applications: a synthetically generated “Raman” data set and a real Raman data set.

3.1. Data set 1—synthetically generated data

A synthetic Raman data set was generated by acquiring real Raman spectra of pure chemical components and normalizing these to Euclidean norm. These spectra formed the A sub matrix in Eq. (1). The B sub matrix was formed by generating four false component images to correspond with each spectral component in B, each weighted so the total intensity of each image component was in the ratio of 2.5:3.5:3.5:1. Fig. 4a shows the spectra profiles used and Fig. 4b shows the false images used.

A and the weighted B matrices were then multiplied and 2% normally distributed random noise was added to the final synthetic data set used in the study. Fig. 5 shows the final data set as “spectra” and as a composite wavelength image.

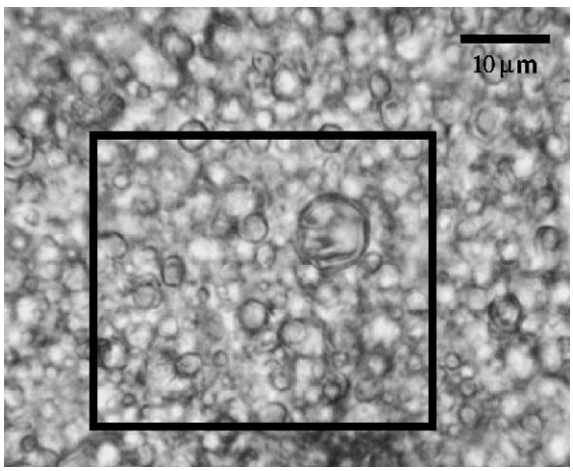

Fig. 6. Visible light image of the emulsion for data set 2. The area in the red box is the 31 μm × 35 μm sample area.

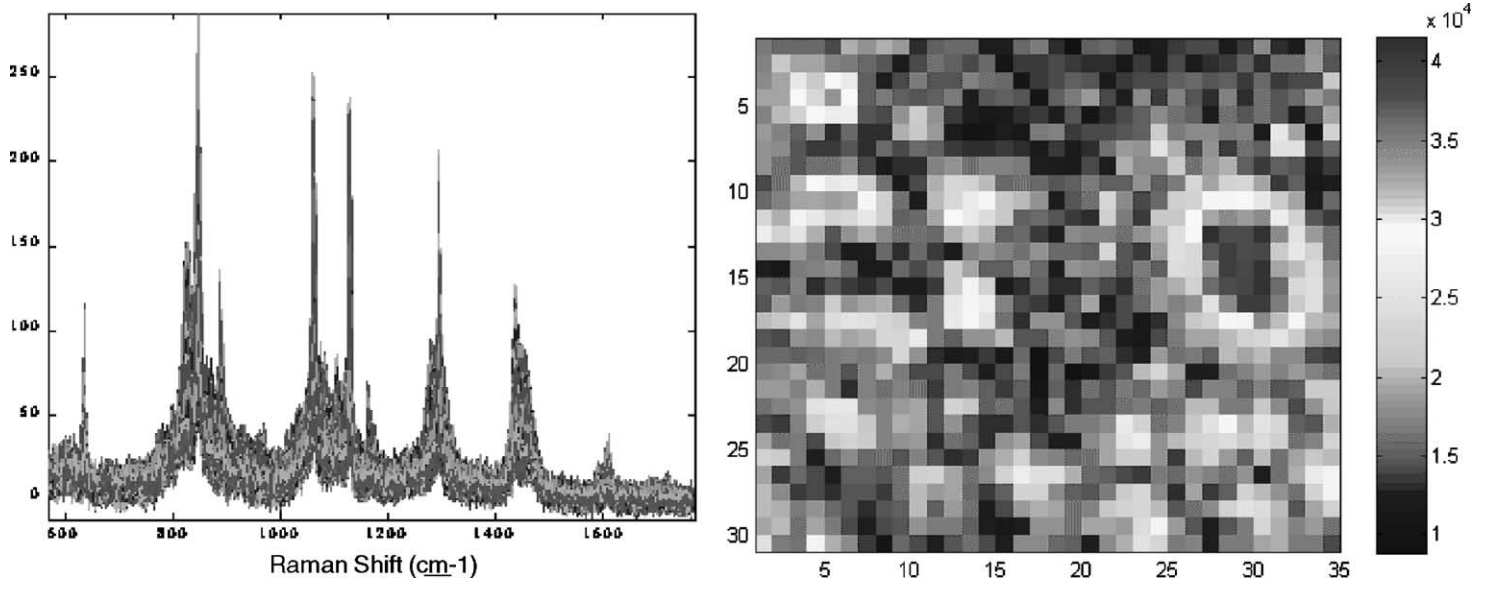

Fig. 7. Overlaid spectra (left) and composite wavelength image (right) of a real Raman image data set. The data set is composed of 1085 × 1200-wavelength spectra for a 31 pixel × 35 pixel image.

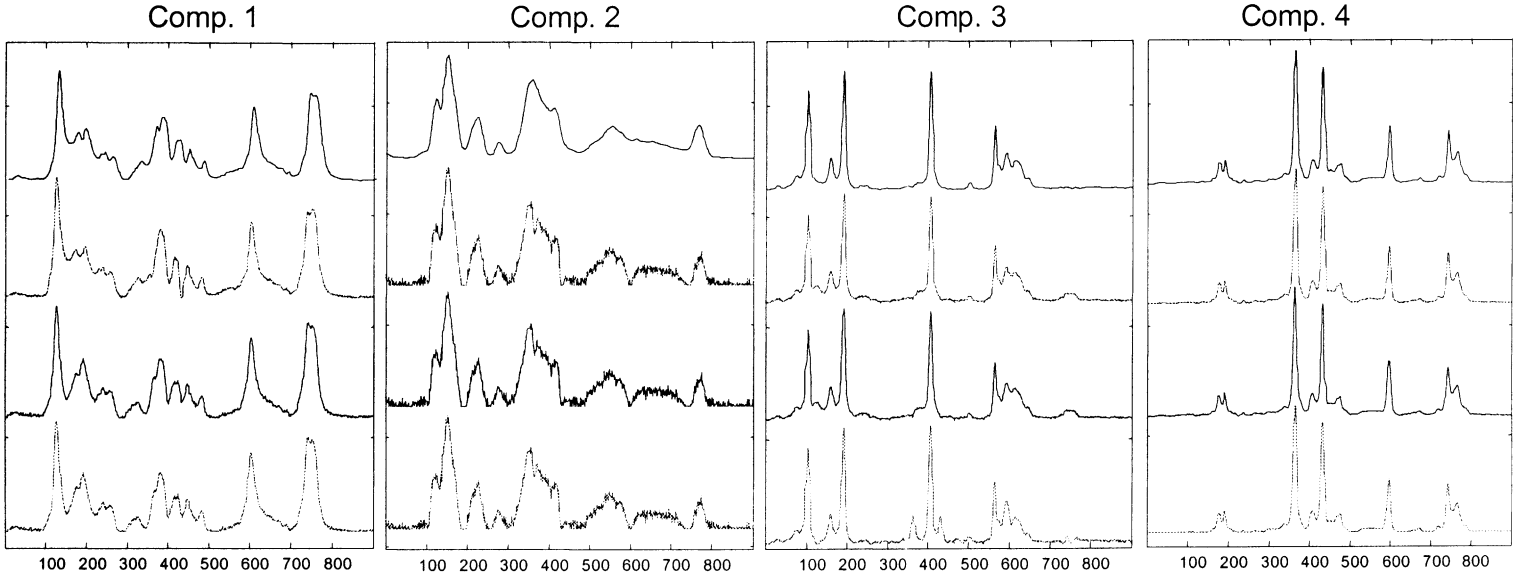

Fig. 8. Resolved "spectral" components for data set 1 (synthetic). The top profiles are those of the original pure profiles, the 2nd, 3rd, and 4th profiles from the top correspond to the MALS, FNNLS, and ALS solution, respectively. *X*-axis is shown as the spectral resolution elements.

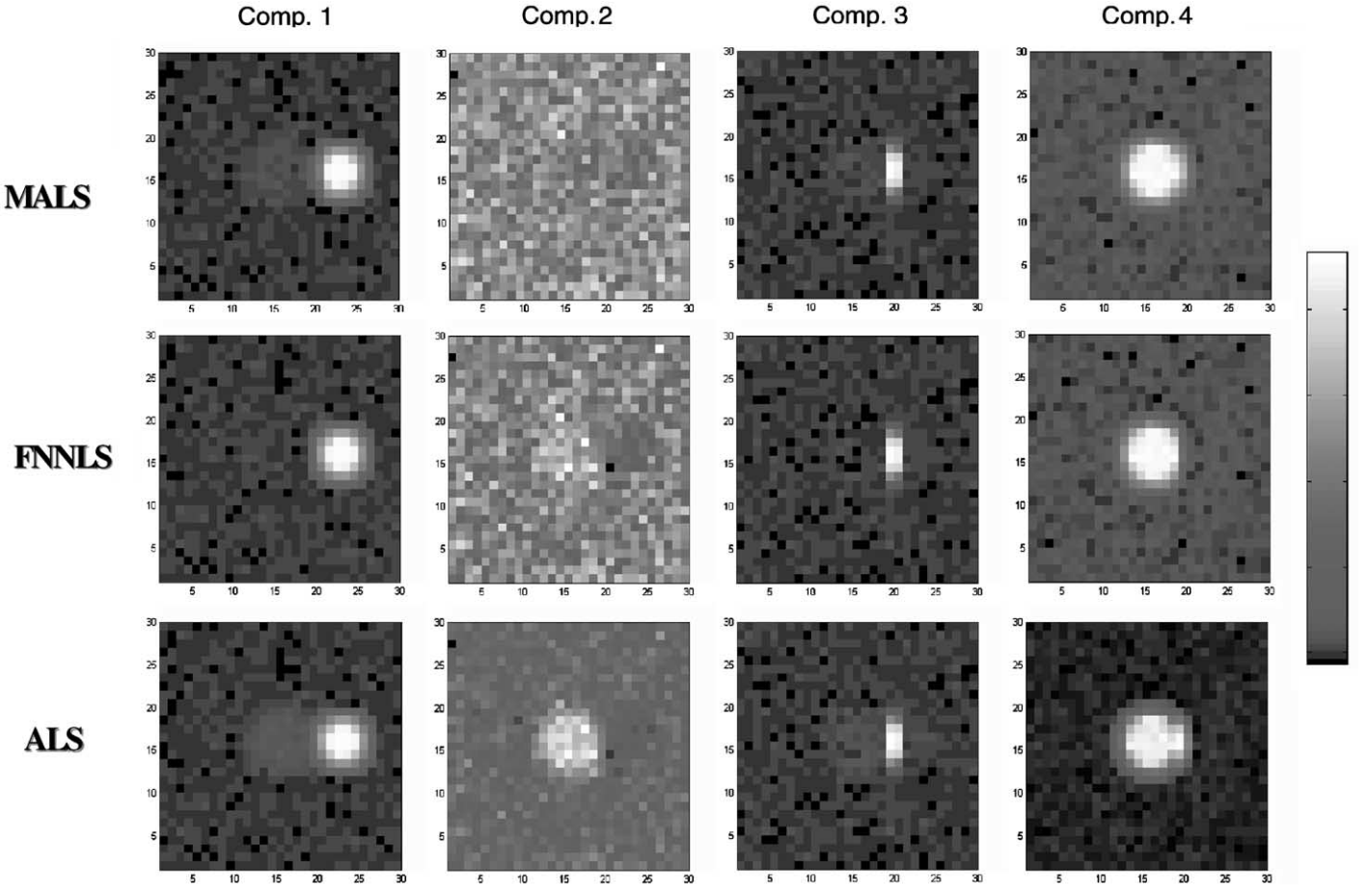

Fig. 9. Resolved “image” components for data set 1 (synthetic). The top, middle, and bottom profiles correspond to the MALS, FNNLS, and ALS solution, respectively. The color scale for these images is in decreasing intensity from red to blue.

3.2. Data set 2—real Raman image data

In previous reports of Raman image analysis work [1,2], SMCR results for oil-in-water emulsion systems were reported. Since our experience with these kinds of systems is fairly extensive and we have a good understanding of the phase behavior and component interaction in these systems, a similar system was used for this study. This particular system was composed of four components (fatty acid, alkyl parabens, glycerol, and ethoxylate ester).

The Raman spectral data was collected by mapping a 31 pixel × 35 pixel area at 1.1 μm intervals in the *X* and *Y* dimensions. A Kaiser HoloScope 785 nm Raman system, optical fiber coupled to a Zeiss microscope, was used for data acquisition. The microscope was equipped with a 100X/0.80 objective. The nominal spectral resolution of the spectrometer was 4 cm^{-1}. The final data set consisted of 1085 spectra of 1201 wavelengths per spectrum for a total of (1.3 million) data points. The CCD exposure time on the Raman system was set to 18 s at each pixel location. The visible light image of the area scanned in the experiment is shown in the red box of Fig. 6. A plot of the spectra and composite wavelength image for the data is shown in Fig. 7.

Preprocessing of the data was kept very simple; spikes were manually removed from the data and a linear baseline correction was applied to remove slope.

3.3. Data analysis

The two data sets described above were analyzed using a single curve resolution software package written by the one of the authors where the only difference in operation was the LS algorithm used in the iterative optimization loop. The software was written in MATLAB and the LS option was chosen by setting an appropriate input flag. The three options chosen for each data set were as follows: (1) a forced-zero-points non-negative ALS, (2) fast non-negative least squares, and (3) MALS with weighting options described in Section 2.3.2 of this report. All analyses were performed on a Dell workstation (PIII-1.2 GHz) with 1 GB RAM.

The goal for the analysis of data set 1 was to see if the *A* and *B* factor space could be successfully extracted from the data and that the optimized solution would converge on a root-mean-squared (RMS) residuals value equal to that added to the original noiseless data (0.0199).

The goal for the analysis of data set 2 was to see if the spectral factor space (*A*) could be extracted from the data set and that corresponding factor image data (*B*) would yield information consistent with how we know the true components concentrations should exist in the emulsion. This information is from experience and could not normally be used in unknown samples.

The RMS error was also measured for each data set in each analysis. These values are useful in comparing performance of each algorithm and in indicating the speed of convergence.

4. Results and discussion

4.1. Data set 1

The curve resolution results for ALS, FNNLS and MALS analysis are shown in Figs. 8–10. The component resolution difficulty should not have been very high for this data set because the spectral and image overlap was not that severe. What made this a difficult problem was the large amount of noise added to the pure data. All methods produced similar results for the spectral profiles although none were able to resolve the noisiest component very well (Fig. 8, component 2). MALS and FNNLS were able to resolve the image information more cleanly than ALS (Fig. 9). Component 2 (high noise) is not cleanly separated

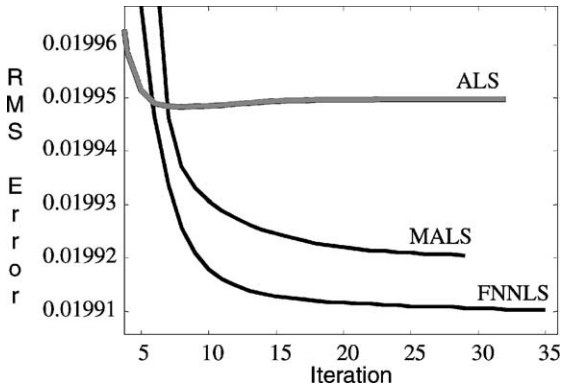

Fig. 10. RMS error with iteration number for data set 1 (synthetic).

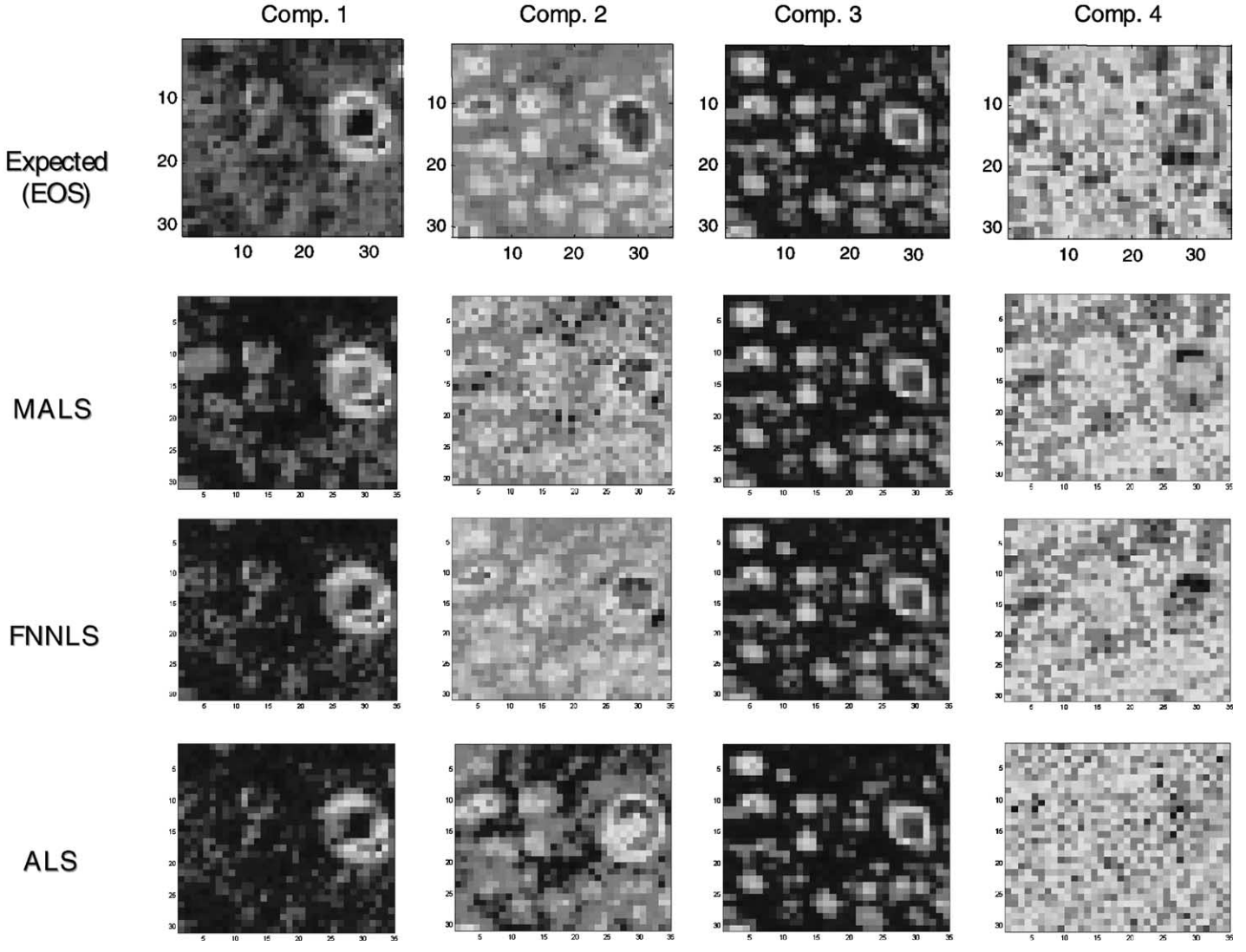

Fig. 11. Resolved "image" components for data set 2 (emulsion data). The top images are those of the expected result as obtained from an EOS analysis. The 2nd, 3rd, and 4th row of images from the top correspond to the MALS, FNNLS, and ALS solution, respectively. The color scale for these images in decreasing intensity from red to blue.

from the other components by ALS and FNNLS and is best separated using MALS. However, for component 1, FNNLS produced the best result. Noise is always a complication in any curve resolution problem. Results from this data set show that even for a relatively straightforward problem noise can degrade results dramatically. If the noise level is high enough, a reasonable solution may not even be possible.

In terms of performance and the ability of each method to find the same minimization point (hopefully the global minimum), the RMS error data show that all three methods performed nearly the same. Fig. 10 shows a plot of RMS error with number of iterations. Again, MALS and FNNLS produce the best results but the difference from that of ALS is negligibly small (0.01992, 0.01991 and 0.01995 for MALS, FNNLS and ALS, respectively). All three methods effectively reach the expected RMS error value of 0.0199. Even thought the number of iterations was nearly the same (29, 35, 32 for MALS, FNNLS and ALS, respectively), the time difference was significant and serves to highlight one of the most important differences between MALS and the other methods. MALS (4.2 s) is an exceptionally fast converging algorithm compared to ALS (21.9 s) or FNNLS (71.2 s) and it can achieve this without loss of accuracy.

4.2. Data set 2

Curve resolution results for data set 2 with ALS, FNNLS and MALS analysis are shown in Figs. 11–13. This data set was chosen because it is a very difficult data set to process. The spectral overlap and component image overlap is very large for several components and this can make the analysis difficult to manage. In addition, the noise level is higher than would be considered ideal although it is still not so large that it renders the problem impossible to solve. In contrast to the first problem, all methods here did not produce the same results. ALS in particular could not satisfactorily resolve image components (Fig. 11) although it did a reasonable job of resolving the first three spectral components. Components 2 (alkyl ethoxylate) and 4 (glycerol) were particularly difficult to resolve because the pixel overlaps and the signal to noise is low. It is interesting to note that none of the methods could accurately resolve the smallest and noisiest component (glycerol). Only the referee method (EOS) was able to fully resolve all the components correctly although MALS performed better than FNNLS. Still, both MALS and FNNLS were able to reasonably resolve the image information. Overall a comparison of each spectral profile and

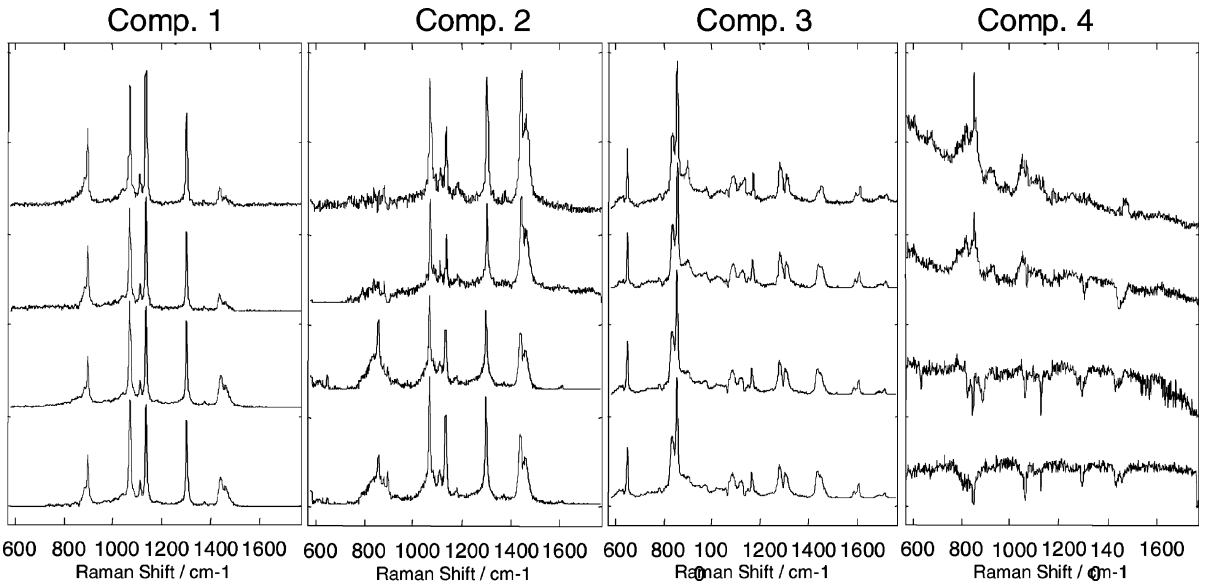

Fig. 12. Resolved spectral profiles for data set 2 (emulsion data): top, expected (EOS result); top middle, MALS; bottom middle, FNNLS; bottom, ALS.

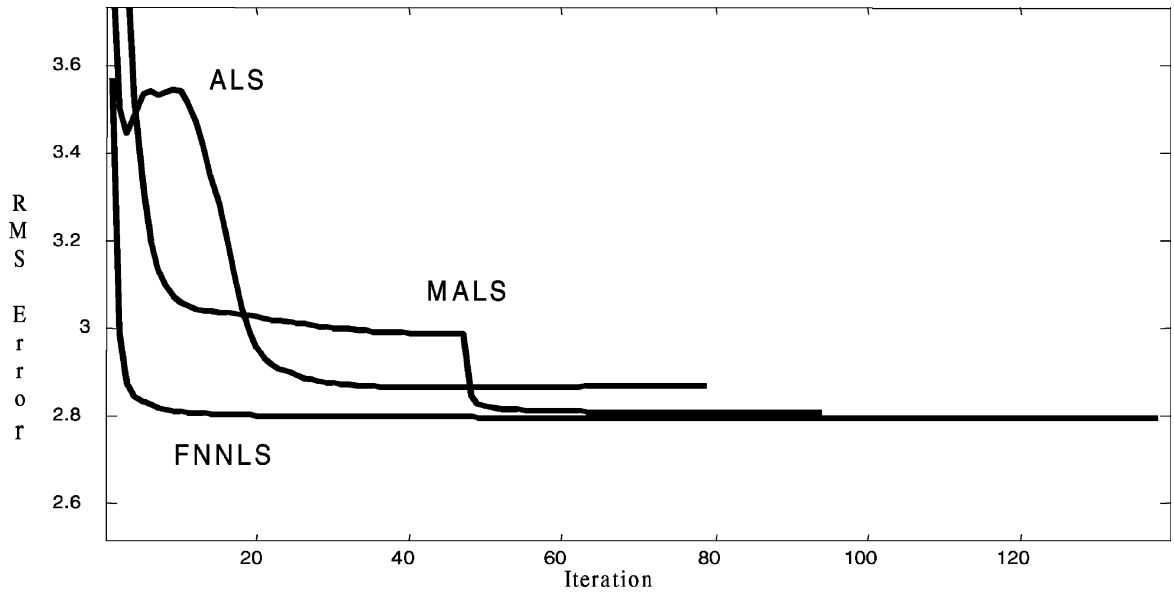

Fig. 13. RMS error with iteration number for data set 2 (emulsion data). The top, middle, and bottom profiles correspond to the MALS, FNNLS, and ALS solution, respectively.

image component shows that for this difficult problem MALS did nearly as well as the referee method. ALS and to a lesser degree FNNLS were not able to do as good at accurately resolving component information.

The RMS error results shown in Fig. 13 show another interesting point that should always be kept in mind when analyzing data using these methods. Even though MALS performed best in resolving component information, FNNLS still achieved the lowest minimum error solution. It is typically assumed that the solution that best minimizes the loss function will inevitably produce the best solution to the problem. This example shows that this is not necessarily so. It is true that the difference in error between MALS and FNNLS is probably not significant (2.808 for MALS versus 2.797 for FNNLS) but it is still large enough to expect a performance benefit by FNNLS. The RMS error for ALS is 2.849 and is not very different from MALS or FNNLS. This does however appear to be significant in term of performance. MALS and FNNLS produce the best results but the difference is negligibly small.

One of the key advantages for MALS is speed. Data set 2 clearly shows what can happen when the data size becomes large and component overlap is high. MALS took less than a minute while FNNLS took over 10 times as long. ALS took less time than FNNLS but still took over four times as long as MALS.

5. Conclusions

Analysis of spectroscopic imaging data is a complex problem that requires different algorithms for different degrees of complexity in the data. Clearly there will always be some methods that perform better than other under specific conditions and for solving particular problems. In the past it was often necessary to make some sacrifice in order to attain results in a reasonable period of time (time and speed for accuracy of result). In addition, availability of different software has always been an issue (and remains so at present). There is still no commercially available software package that provides the necessary range of options required for common curve resolution problems, particularly spectroscopic image analysis.

This study has examined a new method of analysis (MALS) which is capable of addressing these issues. While the results presented here do not represent results for a large number of imaging data sets and

techniques, the results show considerable promise. This suggests that MALS has the potential of providing a common framework for a general curve resolution platform for spectroscopic image analysis and indeed, for most other kinds of component resolution problems. MALS is capable of solving even the most complicated spectroscopic image analysis problem, very quickly, very accurately and in a robust manner. The data presented here show that MALS can be as much as 10 times faster than FNNLS while achieving equal or better convergence properties for real solutions to chemical problems. For extremely large data sets, the time gain in MALS can be significant.

References

[1] W.H. Lawton, E.A. Sylvestri, Technometrics 13 (1971) 617.
[2] J.J. Andrew, T.M. Hancewicz, Appl. Spectrosc. 52 (1998) 790–796.
[3] R. Tauler, D. Barceló, Trends Anal. Chem. 12 (1993) 319–327.
[4] F. Cuesta Sanchez, B.G.M. Vandegiste, T.M. Hancewicz, D.L. Massart, Anal. Chem. 69 (1997) 79.
[5] C.L. Lawson, R.J. Hanson, Solving Least Squares Problems, Prentice-Hall, Englewood Cliffs, NJ, 1995.
[6] R. Bro, S. de Jong, J. Chemom. 11 (1993) 393–401.
[7] J.H. Wang, P.K. Hopke, Chemometrics Intell. Lab. Syst. 55 (2001) 13–22.
[8] P. Paatero, J. Comput. Graph. Stat. 8 (1999) 1–35.